Assessment of the strengthening effectiveness of EBR and NSM techniques for beams' dapped-end by FEM analysis

A.C. Dăescu[1], T. Nagy-György[2], B.G. Sas[3,5], J.A.O. Barros[4], C. Popescu[3,5]
[1]Politehnica University of Timisoara, Romania, cosmin.daescu@ct.upt.ro
[2]Politehnica University of Timisoara, Romania, tamas.nagygyorgy@ct.upt.ro
[3]Norut, NO-8504, Narvik, Norway, cosmin.popescu@tek.norut.no
[4]University of Minho, Portugal, barros@civil.uminho.pt
[5]Luleå University of Technology, SE-97187, Luleå, Sweden, gabriel.sas@ltu.se

Keywords: Numerical analysis; Precast concrete; EBR; NSM; Full-scale tests.

SUMMARY
This document presents the work related to the assessment of the effectiveness of strengthening reinforced concrete (RC) dapped-end beams using carbon fiber reinforced polymers (CFRP). Several non-linear finite element analyses were performed using different strengthening configurations, from the simplest solutions to the more complex ones in which different application schemes were overlapped. The work is focused on evaluating the strengthening systems, considering the ultimate capacities they can lead to and the failure modes involved. There were modeled 17 different strengthening configurations. While some of them provided a marginal increase in the ultimate load that can be applied, several of them provided significant load bearing capacity increase. The observed failure modes ranged from a sudden failure of the whole strengthening system up to the desired progressive failure of the individual components of each strengthening system.

1. INTRODUCTION

The abrupt change of cross-section in a RC structural element results in a complex flow of internal stresses. Such regions are called disturbed regions (D-regions). For RC beams, these regions are called dapped-ends and represent areas where severe reductions of the cross-section are created so that the beam is supported on other structural elements. The load carrying capacity (hereafter capacity, for convenience) of dapped-end beams may be insufficient for reasons such as design errors, code changes, increases in loads or structural damage. Fiber-reinforced polymers (FRP) applied using the externally bonded reinforcement (EBR) or near surface mounted reinforcement (NSMR) techniques, have been proven to be reliable for strengthening RC structures. Several guidelines for strengthening RC structures with FRPs have been published [1-3]. However, these guidelines do not refer in detail to FRP strengthening of dapped-end beams due to insufficient experimental and theoretical investigations on the variations in geometry, material and loading conditions at their dapped-ends. To the authors' knowledge, only four experimental investigations on dapped-end beams strengthened with FRPs have been reported [4-7].

Gold et al. [4] strengthened with FRP several dapped-end beams of a three-story parking garage that were deficient in shear capacity. Due to the lack of design provisions at that time, they carried out a series of tests to verify the effectiveness of the FRP strengthening, as well as the predictive performance of their design approach. The FRP strengthening systems doubled the capacity of the beams, confirming their effectiveness.

Taher [5] assessed the effectiveness of the following techniques for improving the capacity of dapped-end beams: externally bonding steel angles; anchoring unbonded steel bolts in inclined, pre-drilled holes; externally applying steel plate jackets; and wrapping carbon fiber around the beam stem. Tests with 50 small-scale rectangular beams indicated that the FRPs were the most viable solution for strengthening/retrofitting applications. Using the strut and tie analogy, Taher [5] also derived a regression model to estimate the capacity of the FRP-strengthened dapped-end beams, which reportedly provided "reasonable predictions" [5], but he did not consider any possible scale effects of the beams tested for deriving the model.

Tan [6] experimentally investigated the efficiency of several FRP configurations for strengthening dapped-end beams with deficient shear resistance, varying in both fiber types and mechanical anchorage systems for the FRPs. The results showed that glass fiber reinforced polymers (GFRP) provided greater improvements in terms of ultimate capacity than carbon FRP plates and carbon fiber fabrics. He has also verified that the tested mechanical anchorage devices provided higher exploitation of the FRP systems' strengthening capacity by preventing their debonding. The empirically based strut and tie model he derived was applied to predict the shear capacity of the dapped-end beams and proved to be sufficiently accurate for the tested beam types.

In a series of tests, Huang and Nanni [7] verified if the FRPs can increase the capacity of dapped-end beams with "mild steel and no mild reinforcement" [7] and proposed a method for strengthening dapped-end beams with FRPs, which was found to be "satisfactory and conservative" [7].

The current study presents a parametric study of the FRP strengthening systems used for a real case application, previously presented in [8]. The analysis is carried out by means of FEM-based material nonlinear numerical simulations. In several dapped-end beams, diagonal cracks were observed starting at the re-entrant corner, see [8]. These damaged dapped-ends were retrofitted with CFRPs plates. The aims of the strengthening solutions were to increase the capacity up to the design load and to delay the yielding initiation of the steel reinforcement. Three full scale laboratory tests and material nonlinear numerical simulations of those tests were carried out to verify the capacity of the retrofitted dapped-ends. The results showed that FRPs can be used successfully for rehabilitating dapped-ends. However, that study revealed also that the capacity gain is influenced by the application direction and type of FRP material used. This investigation aims to clarify the contributions of individual components of the strengthening and identify the most effective FRP-based strengthening system for the retrofit of large dapped beams ends. The efficiency is discussed in terms of ultimate capacity and global failure mode of the strengthened elements.

2. THE FIELD APPLICATION

The field work was carried out in 2003. In an industrial hall, 20 m span identical precast/prestressed beams with dapped-ends were designed for a reaction force of 800 kN positioned 400 mm from the re-entrant corner. Due to a construction error, in 7 beams the position of the reaction force was displaced by an additional 275 mm, thus diagonal crack formed starting from the re-entrant corner. Considering the new lever arm (675 mm), a deficit in capacity of 200 kN resulted. To increase the demanded capacity and prevent further cracking at service, a strengthening solution using EBR CFRP plates was applied. Based on the initial studies performed in 2003 using a linear FEM and strut-and-tie models, it resulted the necessity to strengthen the dapped-ends with the System 1 (see table 1) in $0^o/90^o$ layout, since this layout provided the longest anchorage length and debonding could have been avoided. In the design of the retrofitting, the strains in FRP were limited to 4 ‰, according to fib Bulletin 14 [1]. However, in the real field application, in some cases, the dapped-ends were arranged head-to-head and the purlins obstructed the application of this layout, hence for these situations the $45^o/90^o$ layout was adopted.

3. EXPERIMENTAL PROGRAM

To verify the efficiency of the applied strengthening configurations, two beams were casted and tested in laboratory environment, each with two dapped-ends. The arrangement, spacing, diameter and strength class of the reinforcements were identical to those of the original beams. The dapped-end specimens were subjected to a monotonic force in increments of 50 kN.

The first element (denoted C1 in [8]) was tested up to failure, serving as reference specimen. The remaining three dapped-ends (denoted C2, C3 and C4 in [8]) were tested up to 800 kN, which corresponded to the design load of the original dapped-ends. These pre-cracked elements were strengthened in three different solutions. The test setup was identical for both the unstrengthened (C) and retrofitted (RC) specimens (see figure 1a).

Two strengthening systems were composed of CFRP plates, applied in 45º/90º (RC2 in figure 1b) and 0º/90º (RC4 in figure 1b) directions, respectively. These strengthening systems were used in the real field application. The overall behavior of the elements retrofitted with these two systems was similar. Both capacity and stiffness increased compared with C1, and crack formation was delayed. At a load of 800 kN, the maximum strains measured in the steel reinforcements in RC2 and RC4 were 31%, respectively 15% less than the strains at this load in the reference specimen. The elements' failure occurred by successively peeling-off of the plates in both situations [8].

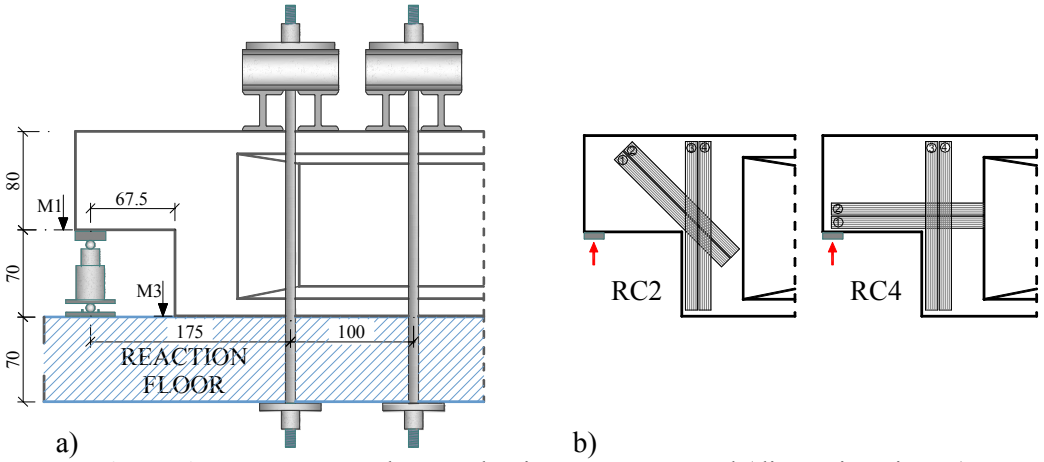

Figure 1: Test set-up and strengthening systems tested (dimensions in cm).

4. NUMERICAL ANALYSIS

The modeling strategy is identical to the one presented in [8], where a very good agreement was found between experimental and numerical results. The standard incremental and iterative Newton-Raphson method for material nonlinear structural analysis was used in the numerical simulations, based on the finite element method. The specimens were modeled with a mesh of 8-node serendipity plane stress finite elements. A Gauss integration scheme with 2x2 integration points was used for all the concrete elements. The steel bars, NSMR, CFRP plates and CFRP fabrics were modeled with 2-noded perfectly bonded embedded truss elements (one degree of freedom per node) [9]. Details regarding the geometry and layout of the reinforcement are given in [8]. Also in this paper, due to the fact that the whole element was modeled in 2D, the out-of-plane effects (such as lateral debonding of the CFRP plates or NSMR) cannot be recorded. For this reason, all the applied CFRP materials are considered to be mechanically anchored so that a maximum capacity could be obtained. Hence the debonding process is disregarded and the capacity relies on the tensile strength of the FRPs.

4.1 Modeling strategy

The numerical analysis presented in this paper was carried out using ATENA software. It is a continuation of the analysis presented in [8] and aims to highlight the performance of the different

FRP strengthening systems that have not been tested nor applied in [8]. To model the optimum strengthening system, the numerical modeling was carried out in two steps.

First, the individual components (P00, P45 and P90 in figure 2) are modeled separately so that their efficiency is determined. The denomination used reflects the angle that the specific strengthening system makes with the longitudinal direction of the beam. For example: P00 means horizontally applied CFRP plates, F45 stands for 45^o applied CFRP fabrics and N90 indicates a vertically applied NSMR bar. The scope is to identify how individual CFRPs perform function of the: (1) applied inclination with respect to the horizontal axis and (2) type of the composite used, i.e. fabrics (F), plates (P) and NSMR (N). The inclinations of 0^o/45^o/90^o were chosen in such a way that they correspond to the real case application and to the experimental program carried out in [8]. Then, fabrics and NSMR components, designed to be equivalent in nominal strength along each direction with the P00, P45 and P90 components were modeled (see models F00, F45, F90, N00, N45 and N90 in figure 2). The mechanical materials properties of the fabrics and NSMR were chosen so that they are similar to the ones used in the real application and experimental testing (see table 1). Due to practical limitations, the resulted values of the nominal strength are not identical, however the difference is marginal (4%). The results of the first step were evaluated and, in the second step, the individual components were combined so that strengthening systems are formed.

Table 1: Mechanical properties of CFRPs (specified by the producer).

System	***FRP***	***Tensile Modulus***	***Strain at failure***	***Thickness***	***Width***	***No. of plates/ layers/ bars***	***Equivalent tensile strength [kN]***
		E [N/mm^2]	***ε_u [‰]***	***t [mm]***	***b [mm]***		
1	Plate (P)	165000	17	1.2	100	2	673
2	Fabric (F)	231000	17	0.17	340	3	680
3	NSMR (N)	165000	13	10	10	3	645

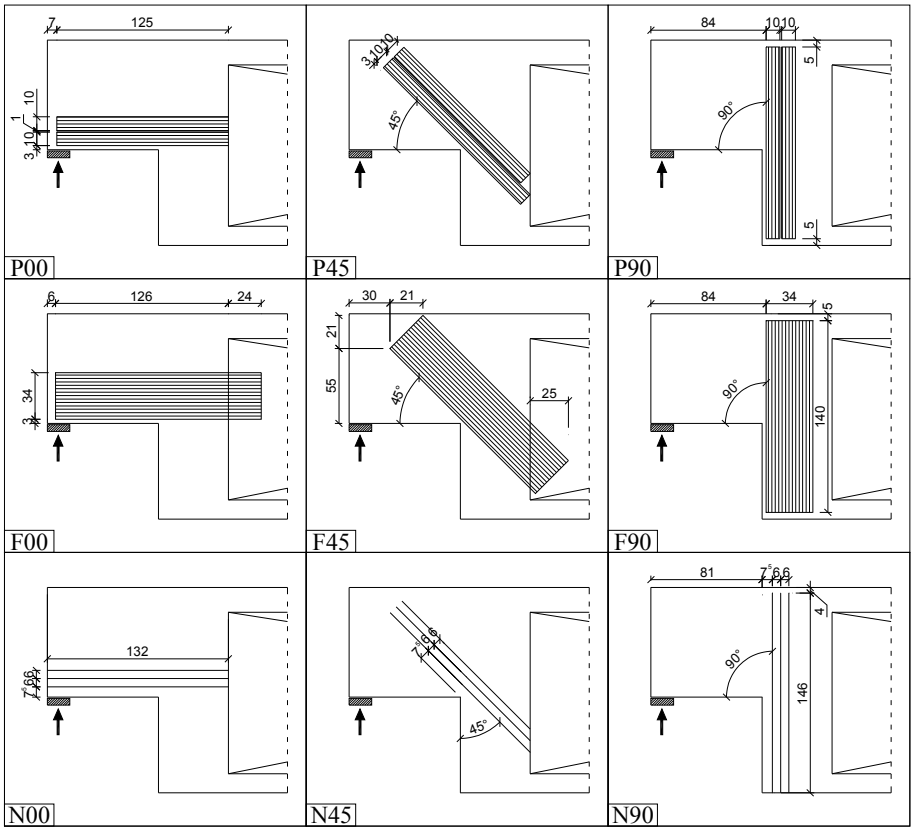

Figure 2: Individual strengthening solutions (dimensions in cm).

4.2 Material characteristics

4.2.1 Concrete

The constitutive model for concrete used in the analysis is a fracture-plastic model that combines constitutive sub-models for tensile and compressive behavior, as presented in the ATENA user manual [9]. This fracture model employs the Rankine failure criterion and exponential softening, with the hardening/softening plasticity component based on the Menétrei-William failure surface [10]. The concrete post-cracking tensile behavior was simulated by the softening function illustrated in figure 3, in combination with the crack band theory [10]. In figure 3, f_{ct} is the tensile strength of concrete, G_f is the mode I fracture energy of concrete and w_c is the crack opening at the complete release of stress, as described in [10]. The concrete had a maximum aggregate size of 16 mm and mean compressive cube strength of 56 N/mm^2, corresponding to a C40/50 concrete strength class.

4.2.2 FRP and steel bars

Discrete bars were used to model the reinforcement; the characteristic behavioral curves are presented in figure 3b. After the peak tensile strength (f_u), the stress was reduced to 10% of f_u so that internal stress redistribution could be assured in the numerical computations. The values used for defining the stress-strain relationships are given in table 1 and table 2. For the NSMR, the thickness, as referred in table 1, represents the depth embedded into the concrete cover, noted as "t" in figure 4.

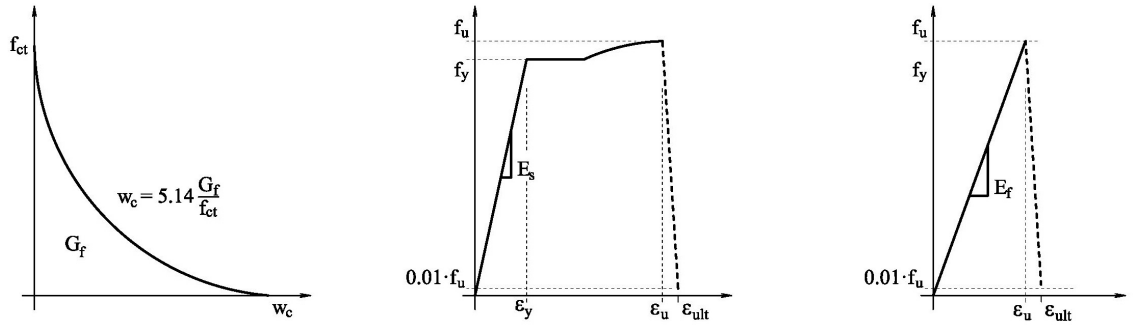

a) Concrete tensile softening diagram. b) Steel reinforcement model. c) CFRP tensile diagram.

Figure 3: Material models used in the numerical analysis.

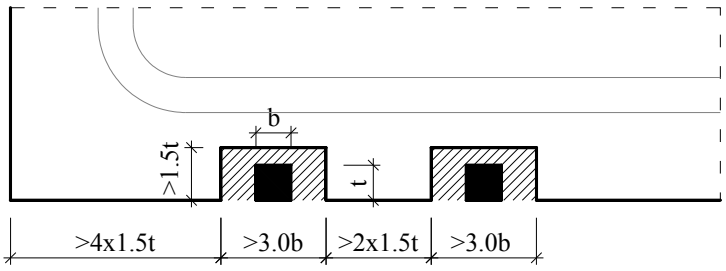

Figure 4: NSMR layout rule according to [3].

Table 2: Properties of the steel material determined in laboratory tests (see also figure 3b).

Diameter ***Φ [mm]***	***Yield strength*** ***f_y [N/mm^2]***	***Tensile strength*** ***f_u [N/mm^2]***	***Yield strain*** ***ε_y [‰]***	***Ultimate strain*** ***ε_u [‰]***	***Strain at failure*** ***ε_{ult} [‰]***
10	780	922	3.6	14.9	15.5
12	522	600	2.5	23.1	24.0
16/18/20	460	600	2.2	19.9	21.0
25	440	625	2.2	18.9	20.0

The behavior of the CFRP was modeled as linear elastic up to failure. In order to avoid numerical integration problems, the post-peak behavior was modeled so that the residual stress is 1% of the maximum tensile strength, see figure 3c. The FRP fabrics were introduced using several discrete lines (modeled as bars perfectly bonded to the substrate), each equivalent to a 50 mm wide strip. The same

procedure was used for the plates, except that the strips were 25 mm wide. In the case of the NSMR, each line was equivalent to the effective cross-section of each individual NSMR bar. The layout of the NSMR reinforcement respects the prescriptions presented in [3]; these rules are schematically presented in figure 4. The predictive performance of the numerical simulations of the experimentally tested elements (see [8]) showed that this approach is reliable since it was capable of capturing the relevant features recorded experimentally. A general view of the finite element model is shown in figure 5.

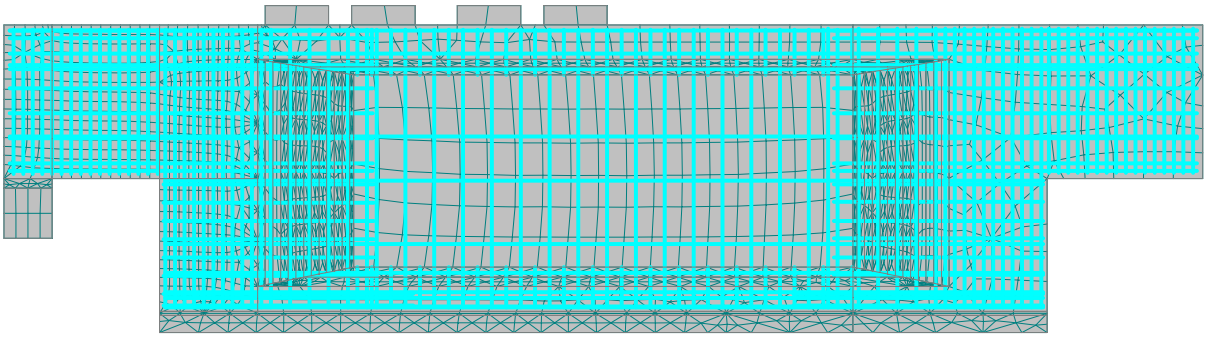

Figure 5: Finite element mesh.

4.3 Boundary conditions

Contact elements without tensile capacity were adopted for the contact of the specimen with the supporting RC floor, thus allowing the eventual separation of the bottom surface. The elastic deformation of the test setup was calibrated based on the experimental results obtained for the reference specimen, and then integrated in all numerical simulations (see [8]).

4.4 Utilization of the individual components

The notations in the following figures are accompanied by the maximum force applied and their percentage increase with respect to the reference specimen C1.

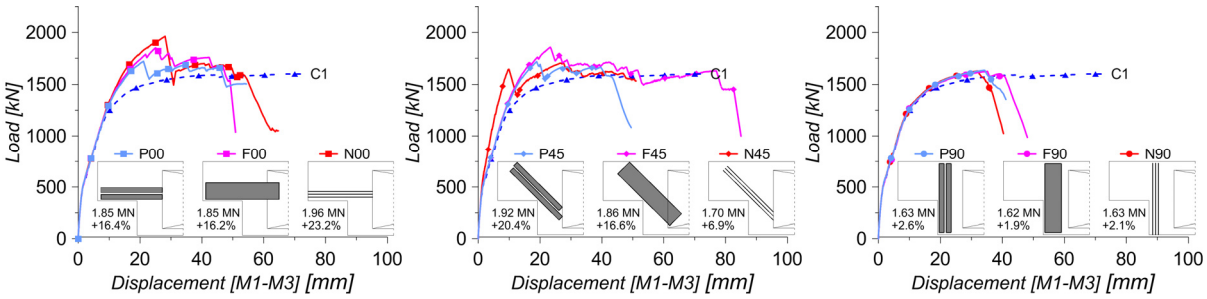

a) 0° angle. b) 45° angle. c) 90° angle.

Figure 6: Load displacement diagrams for individual components of the strengthening systems.

Figure 6 shows the load displacement response obtained from numerical analysis of the individual components applied at 0° (figure 6a), 45° (figure 6b) and 90° (figure 6c). From here on, the "displacement" term in the load-displacement diagrams is defined as the difference in values recorded at points M1 and M3 (see figure 1).

For individual FRP components applied at 0° and 45°, the increase in load was in range of 6.9-23.2% compared to the reference specimen C1, which reached a maximum applied load of 1.59 MN (see [8]). However, the 90° strengthening systems does not provide significant improvement in the bearing capacity (around 2.0%, see figure 6c). In the C1 specimen the yielding occurred at the same time in the horizontal and vertical reinforcement. Applying the 90° strengthening systems, yielding of the vertical steel reinforcement was delayed, while in the horizontal steel bars yielding was reached to a similar applied force as in reference C1. Therefore, the behavior is similar. Thus only the strengthening systems made of individual components applied at 0° and 45° were considered further in the study.

In terms of ultimate capacity increase, for the components P00, F00 and N00 (see figure 6a), the values varied between 1.85 MN (16.4%) up to 1.96 MN (23.2%). At peak load, specimens P00 and F00 failed by rupture of the fibers closest to the re-entrant corner followed by a progressive failure of the adjacent fibers. Immediately after peak load, the fibers failed progressively for both systems P00 and F00, respectively. This pseudo-ductile failure mode is attributed to the distribution of the fibers over a larger area, hence stresses are better redistributed. Opposed to this behavior, in the N00 model, the 3 NSM bars have failed in a brittle manner, all at the same load level. However, in this case, it was obtained the highest capacity increase (+23.2%) compared to the reference specimen (C1).

For the components P45, F45 and N45 (see figure 6b) it was recorded an ultimate capacity in the range of 1.70 MN (7.0%) up to 1.91 MN (20.4%), compared to the reference specimen (C1). The P45 and F45 components failed progressively after the peak load, while all three NSM bars of the N45 component failed in a brittle manner immediately after the peak load has been reached. The N45 has provided a significant increase in the stiffness response of the structure due to an effective arrestment of critical crack propagation.

4.5 Assessment of the of the strengthening systems

Due to technological limitations imposed by the small concrete cover thickness, the NSM bars can only be used in combination with either plates or fabrics. The components applied at 90° did not provide any significant gain in capacity therefore those elements were not used in building up the strengthening systems. Considering these limitations, all possible combinations of strengthening are presented in figure 7.

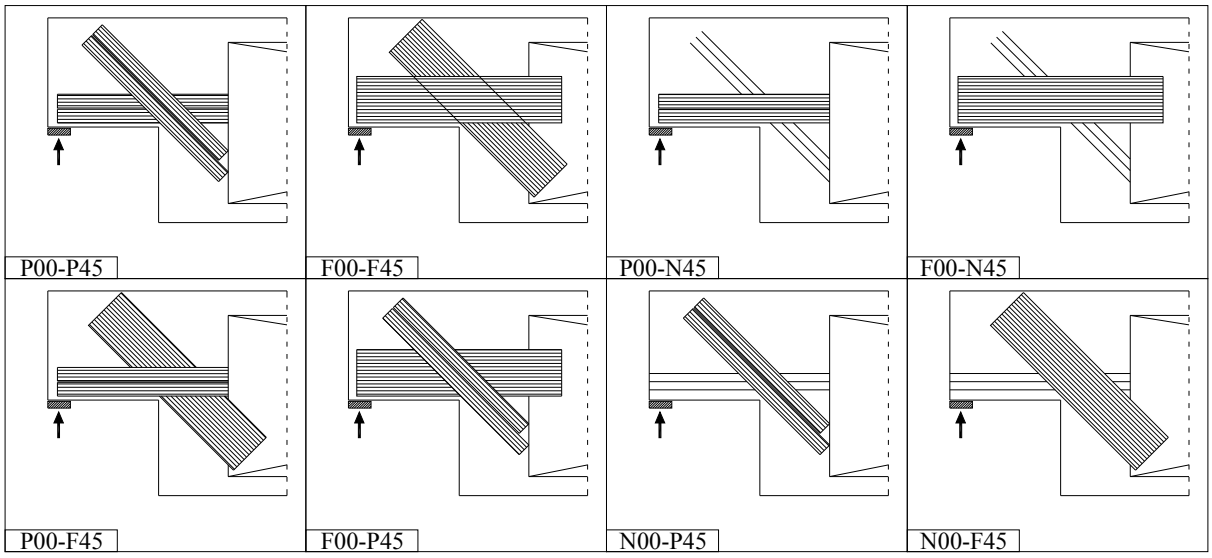

Figure 7: Combined strengthening solutions**.**

In figure 8 are presented the numerical results of the systems components. The notations are accompanied by the maximum force applied and its percentage increase with respect to the reference unstrengthened specimen C1.

In figure 8a-c are shown the load displacement responses for strengthening systems using:
a) plates applied horizontally, in combination with plates at 45°, fabrics at 45° or NSMRs at 45°;
b) fabrics applied horizontally, in combination with plates at 45°, fabrics at 45° or NSMRs at 45°;
c) NSMR applied horizontally, in combination with plates at 45° or fabrics at 45°.

The ultimate capacities of the P00-P45, P00-F45 and P00-N45 systems (figure 8a) are in the range of 1.85 MN up to 2.17 MN (increase of 16.3% 32.3% and 36.2%, respectively). P00-P45 and P00-F45 have a progressive failure of the 45^{o} components, followed by the failure in the first strip of the horizontal CFRP; for P00-F45, at the failure of all the strengthening systems, it was recorded also the

failure of the first stirrup in the main part of the element, next to the re-entrant corner. All the NSMR bars in P00-N45 fail suddenly al the same maximum load.

All models using 00° fabrics (F00-P45, F00-F45 and F00-N45, in figure 8b) reach maximum loads between 1.75 MN up to 2.19 MN (10.2, 35.7 and 37.6%, respectively). For F00-P45 and F00-F45, the failure modes are characterized by the progressive failure of the inclined components, followed by the initiation of the failure in the horizontal strengthening systems. For F00-N45 model, all the 45° NSMR failed suddenly at 1.75 MN together with 3 out of 8 horizontal CFRP strips.

N00-F45 and N00-P45 systems have similar maximum load capacities (1.96 MN, see figure 8c). These loads represent increases of about 23% and 22.8%, respectively. The failure in the both models is brittle; at maximum load, all the NSMR bars fail.

In all the strengthening systems including NSMR bars, the response up to peak load was higher than in the other strengthening configurations and in the C1 specimen.

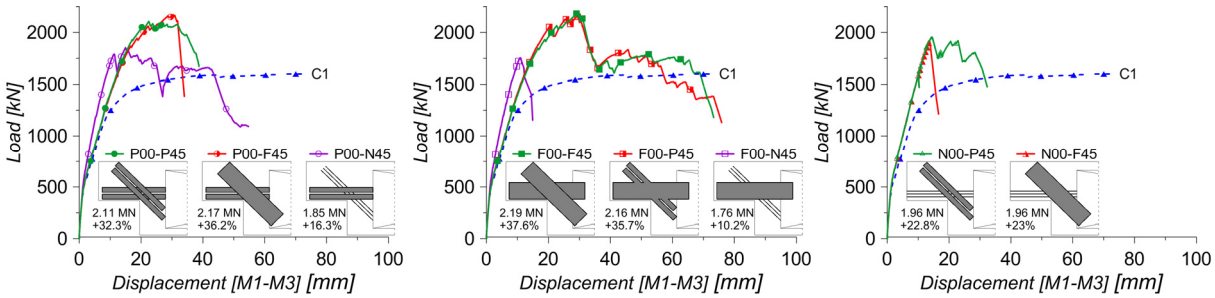

a) P00 as common component. b) F00 as common component. c) N00 as common component.

Figure 8: Load displacement diagrams for strengthening systems.

5. CONCLUSIONS

The study presented in this paper was prompted from a real case study. Several strengthening solutions could have been applied for that field application. However, the initial assessment of the capacity and the choice of the FRP materials available on the market at that time (2003) imposed the use of two different systems for strengthening the dapped-ends on site. To verify the efficiency of the applied systems, a series of tests and numerical simulations were carried out. Since only two strengthening systems were tested, the authors have decided to investigate if these two systems used were the best choice in terms of retrofitting efficiency. Therefore in this paper all practical strengthening configurations that could have been applied were investigated by means of numerical simulations. The modeling approach was first to obtain the individual influence for each component of the strengthening systems used and then to combine these components so that the most efficient strengthening system is determined. Individual models were studied using ATENA software [9], each one having only a part of the strengthening system applied. Then, based on the performance of the individual components, all feasible strengthening systems were built.

The results have showed that all the strengthening systems analyzed provide an increase in the load bearing capacity. While some strengthening systems provided marginal increase with respect to the reference C1 specimen (about 2% for the systems with vertical fibers), many others have provided increased capacities ranging from 6.9 to 37.6% . The optimum solution for strengthening, which would have been chosen, is F00-F45 (fabrics with fibers at horizontal and at 45 degrees) that increased the capacity to about 37.6%. A similar increase was provided by P00-F45 (horizontal plate and fabrics with fibers at 45 degrees), however, in this case, the necessity for mechanical anchorages at the end-plates should be explored. The strengthening system F00-F45 outperforms the two systems used in the field application [8]. The test results for RC2 and RC4, presented in [8] (figure 1b), showed an increase of 20.7% and 16.1% respectivly. The main difference is in the failure modes, which must be

taken into account because a progressive failure mode (F00-F45) is preferred to a brittle one (RC2 and RC4 in the lab tests in [8]).

All the results presented above consider a perfect connection and anchorages between the strengthening systems and the concrete element. However, this limitation is aimed to be further studied and correlated with test results by means of strain distribution in the FRPs with regard to end-plates debonding and intermediate crack debonding.

The results presented in [8] and the numerical analyses presented here show that the applied strengthening systems based on CFRP are viable solutions for improving the capacity of the dapped-end beams, by concentrating a sufficiently strong material as close to the re-entrant corner as possible.

The authors intend to improve their conclusions considering different material properties (i.e. high modulus vs. high strength) or various cross section dimensions for the NSMR, thus generating a future study subject.

REFERENCES

[1] Bulletin 14, Externally bonded FRP reinforcement for RC structures, International Federation for Structural Concrete, (2001).
[2] CNR 200-2004, Guide for the Design and Construction of Externally Bonded FRP Systems for Strengthening Existing Structures, Italian National Research Council, (2004).
[3] ACI 440.2R-08, Guide for the design and construction of externally bonded FRP systems for strengthening concrete structures, American Concrete Institute, (2008).
[4] W.J. Gold, G.J. Blaszak, M. Mettemeyer, A. Nanni, and M.D. Wuerthele, "Strengthening Dapped Ends of Precast Double Tees with Externally Bonded FRP Reinforcement", ASCE Structures Congress, 9, CD version #40492-045-003, (2000).
[5] S. Taher, "Strengthening of reentrant corner zone in recessed RC beams", Eleventh International Colloquium on Structural and Geotechnical Engineering, (2005).
[6] K.H. Tan, "Shear Strengthening of Dapped Beams Using FRP Systems", FRPRCS-5 249-258, (2001).
[7] P.C. Huang and A. Nanni, "Dapped-end strengthening of full-scale prestressed double tee beams with FRP composites". Advances in Structural Engineering, 9, 293-308, (2006).
[8] T. Nagy-Gyorgy, G. Sas, A.C. Daescu, J.A.O. Barros, and V. Stoian, "Experimental and numerical assessment of the effectiveness of FRP-based strengthening configurations for dapped-end RC beams". Eng Struct, 44, 291-303, (2012).
[9] V. Cervenka, L. Jendele, and J. Cervenka, ATENA Program Documentation. Part 1:Theory, Cervenka Consulting Ltd., (2012).
[10] J. Cervenka and V.K. Papanikolaou, "Three dimensional combined fracture-plastic material model for concrete". Int J Plasticity, 24, 2192-2220, (2008).